Supplementary Information

Microfluidic-based wound healing assays for investigating the effects of matrix viscoelasticity on tumor cell migration

Laiqian Ding[a], Zhongyu Wang[a], Xinxin Li[a], Emad Uddin[c], Qingyun Jiang[b], Dexian Sun[a], Juan Wei[d], Li Chen[a], Bo Liu[b], Chong Liu[ae*], Jingmin Li[a*]

[a]Key Laboratory for Micro/Nano Technology and System of Liaoning Province, Dalian University of Technology, Dalian 116024, China.

[b]Department of Biomedical Engineering, Faculty of Medicine, Dalian University of Technology, Dalian 116024, China.

[c]School of Mechanical & Manufacturing Engineering, National University of Sciences and Technology, Islamabad 44000, Pakistan.

[d]Centre for Advanced Laser Manufacturing (CALM), School of Mechanical Engineering, Shandong University of Technology, Zibo 255000, China.

[e]Key Laboratory for Precision and Non-traditional Machining Technology of Ministry of Education, Dalian University of Technology, Dalian 116024, China.

[*]**Corresponding Email:** jingminl@dlut.edu.cn; chongl@dlut.edu.cn

Contents

Supplementary Material S1: Materials and reagents

Sodium alginate and gelatin were purchased from Aladdin Reagent Co., Ltd (Shanghai, China) to prepare hydrogels. Adipic acid dihydrazide (AAD), N-(3-Dimethylaminopropyl)-N'-ethylcarbodiimide (EDC), 1-Hydroxybenzotriazole (HOBt) and MES Buffer (0.1 M, pH 6.5) were purchased from Sigma-Aldrich (Saint Louis, MO, USA). Calcium sulfate ($CaSO_4$), as an ionic crosslinker, was purchased from Aladdin Reagent Co., Ltd (Shanghai, China). PDMS was purchased from Dowing Corporation (Midland-Michigan, USA). SU8-2075 negative photoresist was purchased from Microchem Corporation (Newton, MA, USA). Polymethyl methacrylate (PMMA) plates were purchased from Asahi Kasei Corporation (Tokyo, Japan). Polystyrene (PS) microbeads with a nominal diameter of 1.33 μm and initial density of 0.95 ~ 1.05 g/cm^3 were purchased from Sphere Scientific Corporation (Wuhan, China). Culture medium consists of 89% Dulbecco's Modified Eagle Media, 10% fetal bovine serum, 1% penicillin and streptomycin (Gibco, USA). HeLa cells were purchased from Cell Bank of the Chinese Academy of Sciences (Shanghai, China). Fibronectin (Roche Diagnostics, Indianapolis, USA) was used to improve the adhesion between cells and PDMS substrate. The cell viability was evaluated by using FDA/PI (live/dead, Solarbio, Beijing, China). Doxorubicin hydrochloride (DOX) and dimethyl sulfoxide (DMSO) were purchased from Aladdin Reagent Co., Ltd (Shanghai, China).

Supplementary Material S2: Numerical simulation of drug diffusion through the hydrogel

To investigate how the hydrogel affects the DOX diffusion, a 2D model based on the cross-section geometry for diluted substance transport in the porous media was developed by using COMSOL software (Fig. S1f). For drug treatment, the DOX concentration in the chambers of the liquid introducing layer was set to 1.0×10^{-3} mol/m^3 or 1.0×10^{-2} mol/m^3 (corresponding to 1 μM or 10 μM). The initial DOX concentration in the hydrogel was set to 0 mol/m^3. The interface between the liquid introducing layer and cell culture layer was set as the inflow boundary condition. The diffusion coefficient of DOX in the culture medium was set to 1.0×10^{-10} m^2/s.[1,2] Note that the effects of DOX concentration on the diffusion rate were neglected in the simulation.

References:

[1] S. Shirazi-Fard, A. R. Zolghadr and A. Klein, *New J. Chem.*, 2023, **47**(48): 22063-22077.

[2] O. Degerstedt, J. Gråsjö, A. Norberg, E. Sjögren, P. Hansson and H. Lennernäs, *Eur. J. Pharm. Sci.*, 2022, **172**: 106150.

Supplementary Material S3: Analysis of fluid shear stress in the chambers under two operating modes

Fluid shear stress, as one kind of mechanical stimulus, plays an important role in regulating the behaviors of cells exposed to fluid microenvironment. Considering that the 2D CFD models can not adequately reflect the actual conditions of the flow field in the microfluidic device, the 3D models have been employed to investigate the distribution of fluid shear stress on the bottom of the chamber. The simulation results under different operating modes are shown in Fig. S2a and Fig. S2b, respectively. It is observed that the distribution of fluid shear stress is also axisymmetrical as the midperpendicular of the cross-line A-A' (or B-B') is taken as the axis. When the partition structure is opened, the fluid shear stress comes into being in the wound area, and it is less than that in the chambers according to the color shades. Contrary to the flow speed distribution on the cross section, there is a greater fluid shear stress in the edge than the central region of the chamber (as shown in Fig. S2c and Fig. S2d). In addition, the fluid shear stress profiles along the cross-line A-A' and B-B' are quantitatively analyzed. Both curves of the fluid shear stress contain two similar peaks (about 7.0×10^{-4} dynes/cm^2). The difference between them is that the fluid shear stress along the cross-line B-B' exists a local minimum (about 3.7×10^{-4} dynes/cm^2) in the wound area, whereas there is no fluid shear stress in the corresponding area when the partition structure is closed. The fluid shear stress with the above order of magnitude has no negative impact on the cell growth and proliferation.

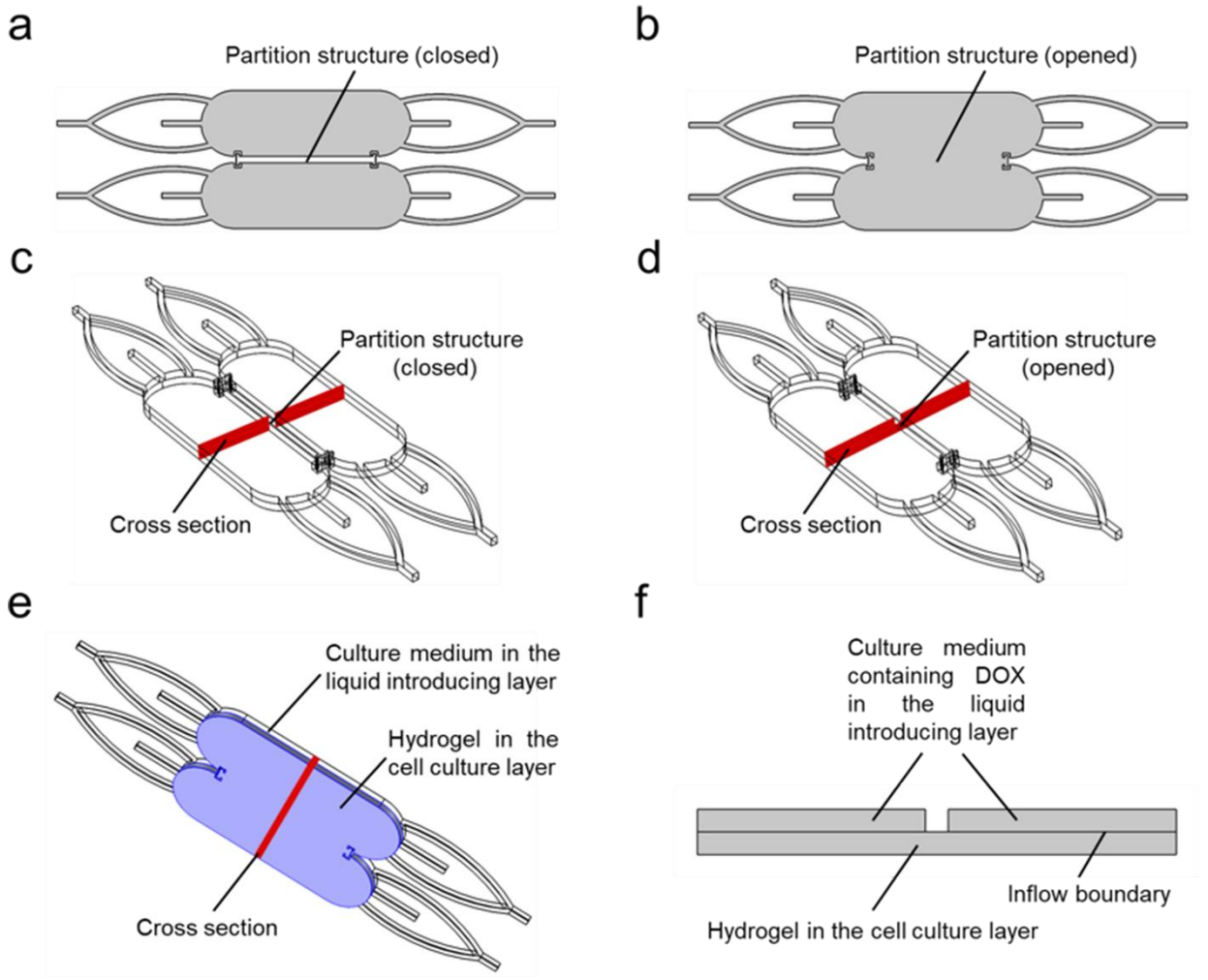

Fig. S1 Schematic of the numerical simulation models for evaluation of the flow fields and drug diffusion in the microfluidic device. The 2D CFD model with a/an (a) closed and (b) opened partition structure before perfusing the hydrogel into the chambers. The 3D CFD model with a/an (c) closed and (d) opened partition structure before perfusing the hydrogel into the chambers. (e) The 3D CFD model with an opened partition structure after perfusing the hydrogel into the chambers. (f) The 2D model based on the cross-section geometry for diluted substance transport in the porous media.

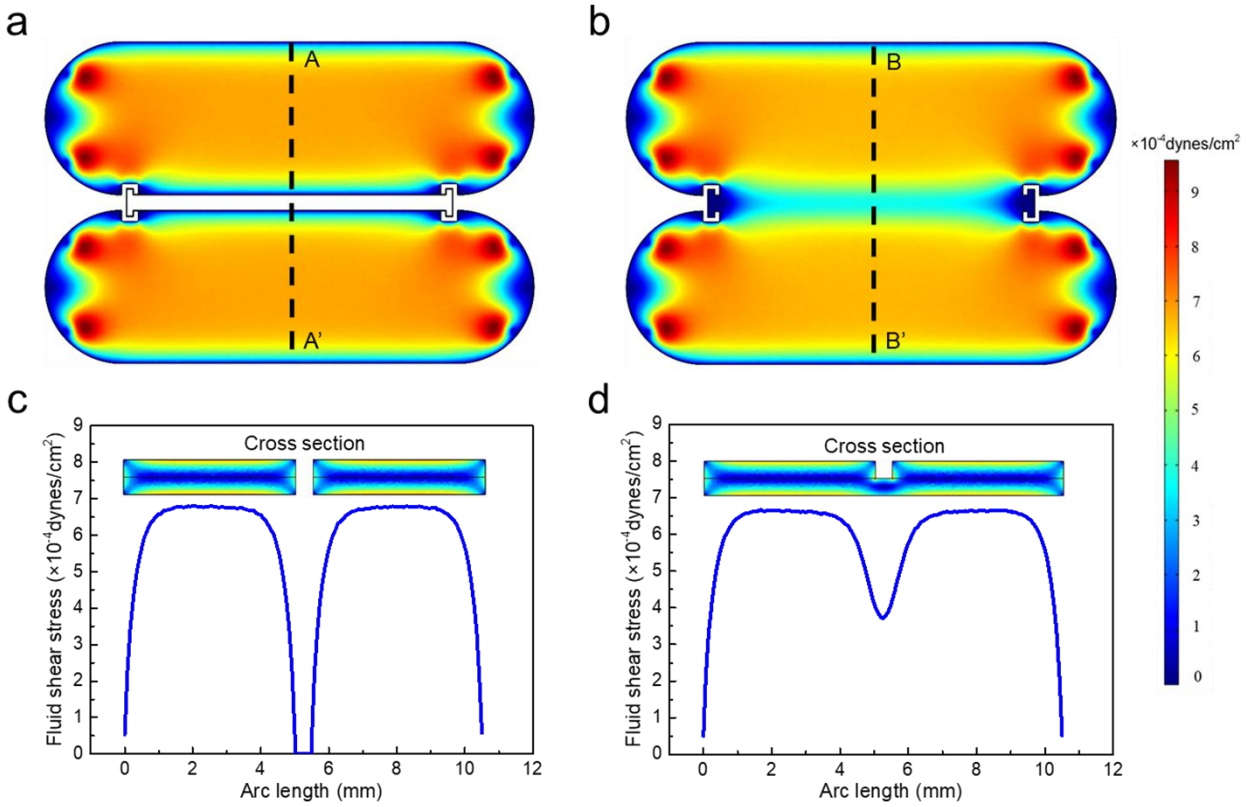

Fig. S2 Steady-state simulation results of the fluid shear stress on the bottom of the chamber in 3D CFD models under two operating modes. The distribution of fluid shear stress on the bottom of the chamber when the partition structure is (a) closed and (b) opened. (c) The fluid shear stress profile along the cross-line A-A' when the partition structure is closed. (d) The fluid shear stress profile along the cross-line B-B' when the partition structure is opened. The embedded cross section in (c) and (d) corresponds to the position of the cross-line A-A' and B-B' in (a) and (b), respectively.

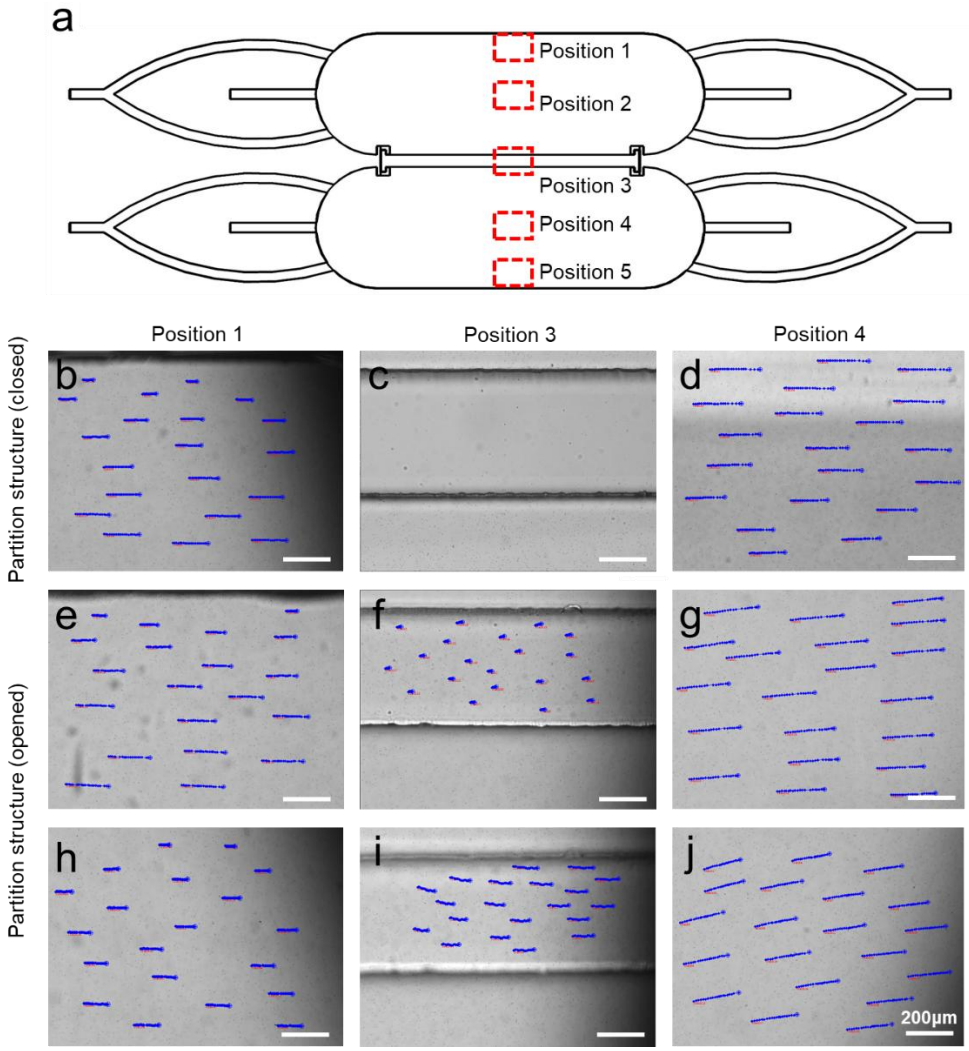

Fig. S3 Results of the flow speed measurement by particle tracking assays. (a) Schematic of five positions (P1, P2, P3, P4 and P5) in the chambers selected to record the movements of PS microbeads. (b)~(d) show the trajectories of PS microbeads in the P1, P3 and P4 along the cross-line C-C' (as shown in Fig. 2c) when the partition structure is closed. (e)~(g) show the trajectories of PS microbeads in the P1, P3 and P4 along the cross-line E-E' (as shown in Fig. 2d) when the partition structure is opened. (h)~(j) show the trajectories of PS microbeads in the P1, P3 and P4 along the cross-line G-G' (as shown in Fig. 2d) when the partition structure is opened.

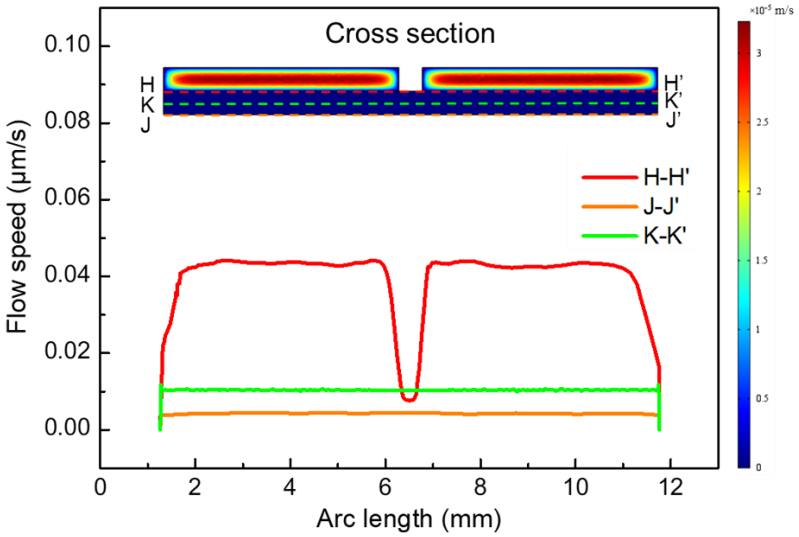

Fig. S4 Steady-state simulation results of the flow speed distribution on the cross section of the chamber after the hydrogel is perfused into the microfluidic device. The flow speed profiles along the cross-line H-H', J-J' and K-K' are exhibited.

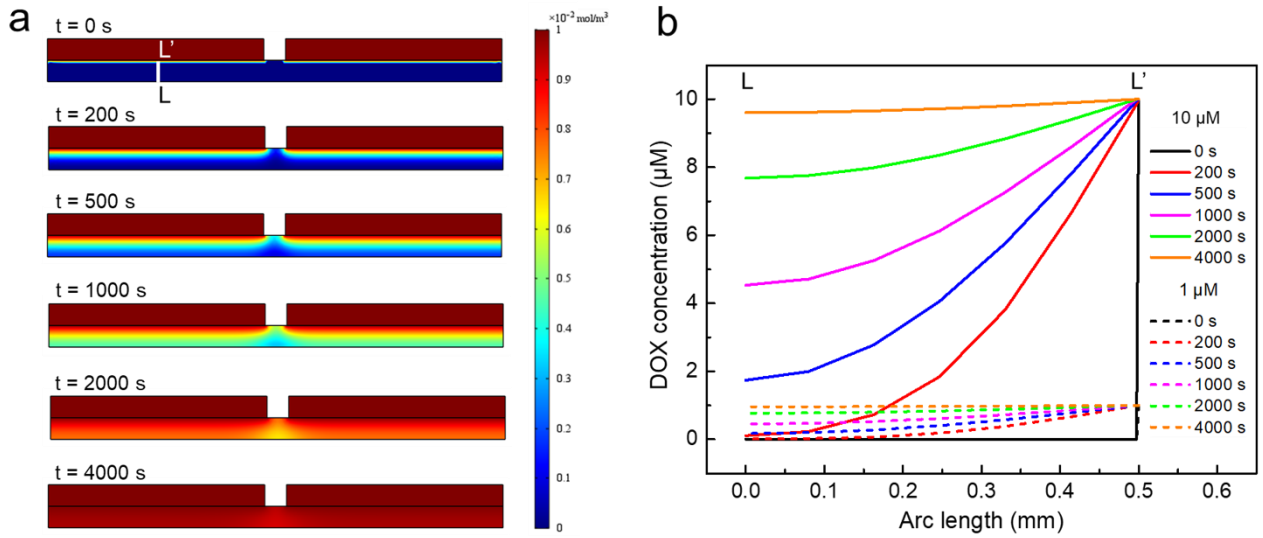

Fig. S5 Simulation results of the DOX diffusion in the hydrogel. (a) The concentration distributions of DOX in the hydrogel at different times when the cells are treated with 10 μM DOX. (b) The changes in the DOX concentration along the cross-line L-L' as shown in (a) over time.

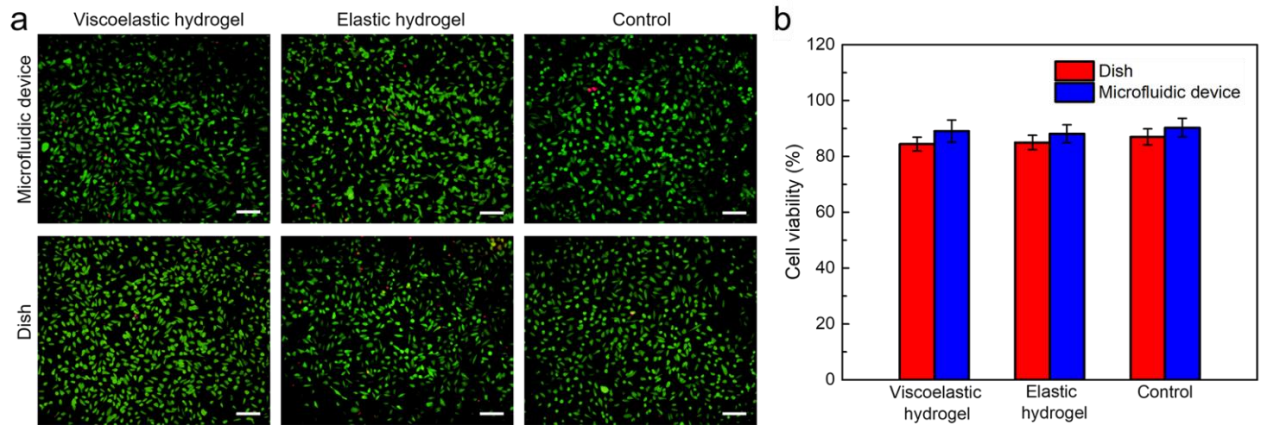

Fig. S6 Cytotoxicity evaluation of hydrogels. (a) The stained HeLa cells cultured in the microfluidic devices and dishes with the extract of viscoelastic hydrogel, extract of elastic hydrogel and culture medium (control), respectively. (b) The cell viabilities in different groups for evaluation of hydrogel biocompatibility (n=5 in each group; About 1000 cells including the living cells and dead cells were counted and analyzed in each repeat). The scale bar in (a) is 100 μm.

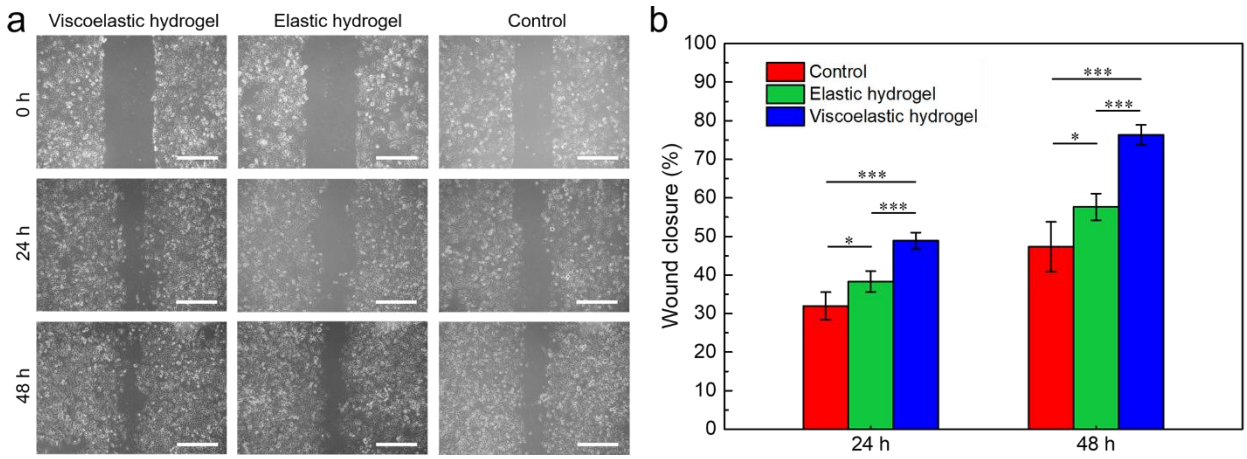

Fig. S7 Results of wound healing assays in the dishes with different mechanical microenvironments. (a) Microscopy images of the wounds exposed to the viscoelastic hydrogel, elastic hydrogel and culture medium (control) at different times, respectively. (b) The wound closure of the monolayer in different groups at 24 h and 48 h; Two-tailed unpaired Student's *t*-test is used for analysis of the data; * indicates statistical significance of $P < 0.05$ (n=5); *** indicates statistical significance of $P < 0.001$ (n=5). The scale bar in (a) is 500 μm.

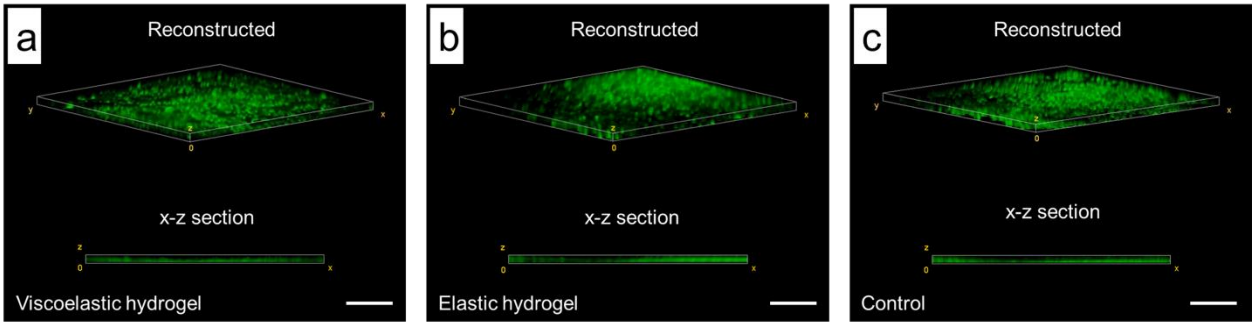

Fig. S8 Reconstruction for cell distributions in the microfluidic device by confocal imaging after 48 h of wound healing assays. The distribution of the HeLa cells covered with the (a) viscoelastic hydrogel, (b) elastic hydrogel and (c) culture medium (control). The scale bar in (a-c) is 100 μm.

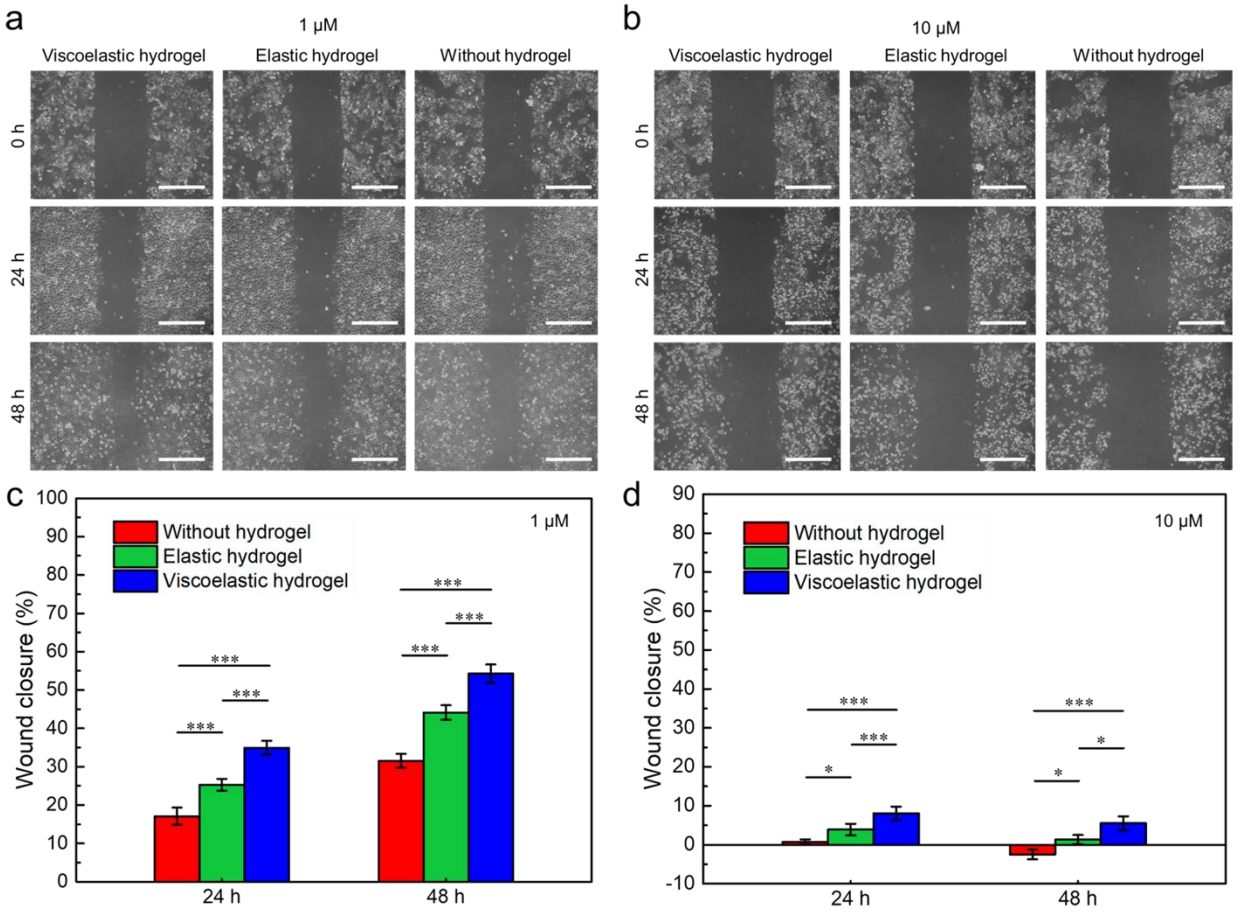

Fig. S9 Results of wound healing assays with DOX treatment in the dishes. Microscopy images of the wounds exposed to the viscoelastic hydrogel, elastic hydrogel and culture medium (without hydrogel) after treatment with (a) 1 μM and (b) 10 μM DOX for different durations, respectively. The wound closure of the monolayer in different groups after treatment with (c) 1 μM and (d) 10 μM DOX for 24 h and 48 h; Two-tailed unpaired Student's *t*-test is used for analysis of the data; * indicates statistical significance of $P < 0.05$ (n=5); *** indicates statistical significance of $P < 0.001$ (n=5). The scale bar in (a) and (b) is 500 μm.